

SCIENTIFIC REPORTS

OPEN

Increase of power conversion efficiency in dye-sensitized solar cells through ferroelectric substrate induced charge transport enhancement

Xiaoyan Liu^{1,2}, Qifeng Zhang³, Jiangyu Li^{4,2}, Nagarajan Valanoor⁵, Xiao Tang¹ & Guozhong Cao⁶

Ferroelectric functionalized dye-sensitized solar cells were fabricated by using a positively-poled LiNbO₃ substrate coated with ITO (ITO-LiNbO₃) as a collector electrode and demonstrated enhanced power conversion efficiency. Surface potential properties of TiO₂ nanoparticle film coated on the ITO-LiNbO₃ (TiO₂/ITO-LiNbO₃) examined by Kelvin probe force microscopy (KPFM) confirmed that a large electric field (a few 10V/μm) generated from LiNbO₃ can penetrate through the ITO layer and is applied to TiO₂ film. This polarization-induced electric field leads to an increased photocurrent density by attracting and promoting electrons to direct transport through the mesoporous TiO₂ network toward the collector electrode and a decreased charge recombination by facilitating electrons to pass through fewer boundaries of nanoparticles, resulting in high power conversion efficiency. The power conversion efficiency was enhanced by more than 40% in comparison with that without polarization-induced electric field. Incorporating functional ferroelectrics into photovoltaic cells would be a good strategy in improving photovoltaic performance and is applicable to other types of photovoltaic devices, such as perovskite solar cells.

The utilization of solar energy becomes increasingly important, as the fossil and mineral sources are not only limited but also the main sources of environmental pollution. Dye-sensitized solar cells (DSCs) are among the most promising low cost photovoltaic devices to substitute silicon solar cells, the latter is the dominant technology used for commercial solar panels at present¹. The practical DSC contains broadly a mechanical support coated with transparent conductive oxides (TCOs) as a collector electrode; semiconductor film, usually TiO₂; a sensitizer absorbed onto the surface of the semiconductor; an electrolyte containing a redox mediator; and a counter electrode capable of regenerating the redox mediator. A nanostructured TiO₂ film with a high surface area can benefit efficient dye loading and create pathways for electron transport^{2,3}. A high photocurrent density as much as 20 mA/cm² can be generated as a result of good light harvesting and electron injection^{4,5}. On the other hand, the nanostructured TiO₂ film with high surface area can also promote charge recombination by decreasing electron diffusion length and hindering charge transport due to the highly random surfaces and boundaries.

Different with the other organic photovoltaic devices, in the DSC the charge generation is done at the TiO₂-dye interface and the charge transport is completed by the TiO₂ and the electrolyte. Sun light is absorbed

¹College of Metallurgy and Materials Engineering, Chongqing Key Laboratory of Nano/Micro Composites and Devices, Chongqing University of Science and Technology, Chongqing, 401331, China. ²Shenzhen Key Laboratory of Nanobiomechanics, Shenzhen Institutes of Advanced Technology, China Academy of Sciences, Shenzhen, 518055, Guangdong, China. ³Department of Electrical and Computer Engineering, North Dakota State University, Fargo, ND, 58108, USA. ⁴Department of Mechanical Engineering, University of Washington, Seattle, WA, 98195, USA. ⁵School of Materials Science and Engineering, University of New South Wales, Sydney, NSW, 2052, Australia. ⁶Department of Materials Science and Engineering, University of Washington, Seattle, WA, 98195, USA. Correspondence and requests for materials should be addressed to X.L. (email: xyliu@cqust.edu.cn) or G.C. (email: gzcao@u.washington.edu)

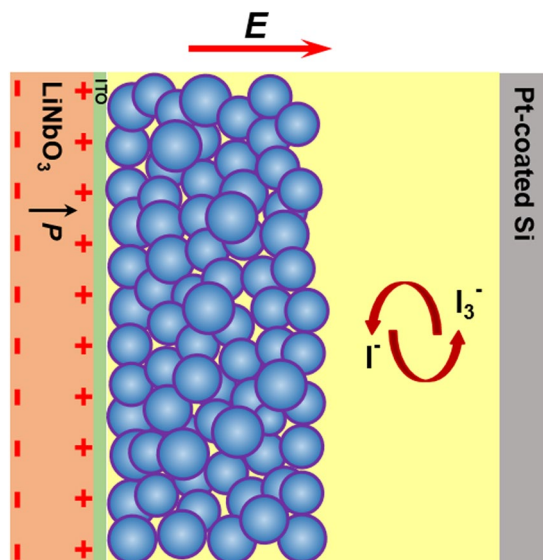


Figure 1. Schematic of DSCs in which ITO coated ferroelectric LiNbO₃ single crystal with positively-poled surface is used as a collector electrode.

by a dye monolayer located at the junction between the nanostructured TiO₂ and the triiodide/iodide (I₃⁻/I⁻) redox electrolyte, leading to an excited sensitizer which injects electrons into the conduction band of the TiO₂. The processes contributing to the photocurrent are the migration of electrons in the TiO₂ film toward the collector electrode, the regeneration of oxidized sensitizers by redox couples in electrolyte, and the regeneration of the redox couples by a reduction occurring at the counter electrode. However, the injected electrons may also recombine either with the oxidized sensitizer or with the oxidized redox couple at the TiO₂ surface, resulting in a loss of cell efficiency. Furthermore, in the DSC the charge transport is mainly forced by electron diffusion because there is no significant electric field existing in the system⁶. Due to trap and recombination limited transport, the electron diffusion through the nanostructured TiO₂ film is much slower than that in the single crystal TiO₂ film^{7,8}. Extensive studies have shown that the rate of recombination depends on both the electron concentration and the film structure, which can be rationalized in terms of an exponential trap distribution model^{9–11}. Enormous progresses have been made through design and synthesis of new dyes¹², semiconductors¹³ and redox couples¹⁴, and optimization of semiconductor morphologies^{3,15}, leading to a great advancement in power conversion efficiency (PCE). However, there is still a big gap between the practically achieved PCE and the theoretical maximum achievable one (~30%)¹⁶. Improving the charge transport has become one of the most important issues for approaching a higher efficiency of DSCs.

Recent years, ferroelectric materials have attracted extensive attention for solar cells owing to their unique surface/interface charge properties attributed to spontaneous polarization. The integration of ferroelectrics was initially done with polymer solar cells (PSCs). Yuan *et al.*¹⁷ and Nalwa *et al.*¹⁸ obtained an enhanced PCE by introducing a ferroelectric polyvinylidene fluoride (PVDF) layer into PSCs, the former demonstrated an increased open-circuit voltage (V_{oc}) resulting from an internal electric field ensured by the ferroelectric polymer layer and the later verified an enhanced photocurrent density (J_{sc}) and fill factor (FF) owing to enhanced exciton dissociation by the local electric field of ferroelectric dipoles. Lan *et al.*¹⁹ observed an increased PCE from inverted PSCs by adopting a dual phase SrTiO₃/ZnO nanocomposite films as a cathodic buffer layer and claimed that spontaneous polarization of SrTiO₃ induce a self-built electric field to impede charge recombination at the interface of the active layer and buffer layer. By applying BaTiO₃/TiO₂ nanocomposite films as photoanodes, our recent work² demonstrated enhanced PCEs in the DSCs. We concluded that performance improvement in BaTiO₃ nanocrystalline incorporated cells was due to the increase of electron mobility and decrease of charge recombination caused by the local electric field of ferroelectric BaTiO₃ dipoles. Moreover, in perovskite solar cells, ferroelectric polarization was demonstrated to improve charge separation inside the absorber and to promote charge transport from CH₃NH₃PbI₃ to TiO₂²⁰, resulting in enhanced photovoltaic performance.

In this paper, we propose a design of ferroelectric functionalized DSCs using a positively-poled (+Z) LiNbO₃ substrate coated with ITO (ITO-LiNbO₃) as a collector electrode. Figure 1 illustrates the schematic of the proposed device. After poling, LiNbO₃ single crystal exhibits a large spontaneous polarization ($P \sim 75 \mu\text{C}/\text{cm}^2$) along the crystallographic Z-axis²¹ which generates high density bound charges at the surface^{22,23}. When the poled surface of LiNbO₃ single crystal is deposited with an ITO layer followed by the coating of a TiO₂ nanoparticle film, the bound charges at the poled surface are partially or completely compensated by the ITO, and the screening charge sheet generates an electric field penetrating into the nanostructured TiO₂ film. It is worth mentioning that, at the interface of ITO-LiNbO₃ and nanostructured TiO₂ film, the polarization-induced charges will not be fully compensated by the low-concentration free charges in semiconductor, which leads to the formation of an uncompensated internal field in the TiO₂ nanoparticles. Such a polarization-induced electric field is anticipated to favor charge transport in DSCs. LiNbO₃ single crystal is employed for this study because of its advantages in

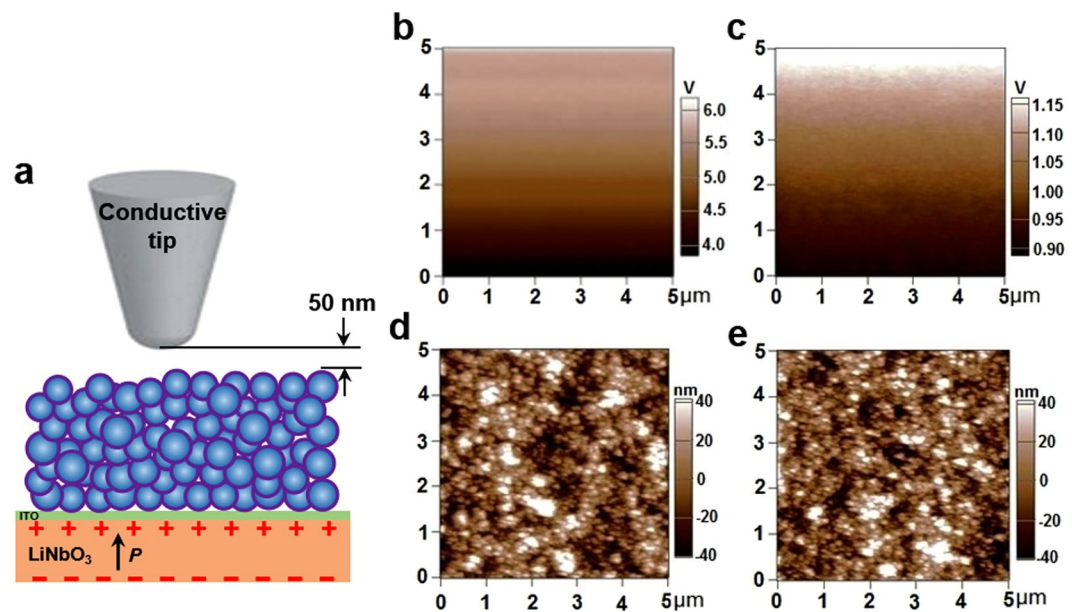


Figure 2. (a) Schematic of the Kelvin probe force microscopy (KPFM) measurement. Surface potential images of TiO₂/ITO-LiNbO₃ (b) and TiO₂/ITO-glass (c). Topographic images of TiO₂/ITO-LiNbO₃ (d) and TiO₂/ITO-glass (e). The images (b–e) were taken after subjected to the sintering process.

material characteristics such as (1) the possession of a large spontaneous polarization (P) of $75 \mu\text{C}/\text{cm}^2$ arising from the ionic displacements within the crystal lattice, which is highly stable due to a large coercive field (21 kV/mm, the electric field for polarization reversal of congruent LiNbO₃), resulting in a permanent polarization without change of orientation and magnitude, and (2) its high Curie temperature (1140 °C, the phase transition point from paraelectrics to ferroelectrics) which enables to maintain ferroelectric properties through a sintering process at the temperature ranging of 350–500 °C to form a mesoporous TiO₂ network that provides pathways for charge transport. In addition, non-doped congruent LiNbO₃ single crystal shows a good optical transmittance in the visible region (Figure S1). In our work, by using the ITO-LiNbO₃ (+Z) as a collector electrode, the PCE of DSCs increases by 42.9% resulted from both increased photocurrent density (J_{sc}) and fill factor (FF). The possible mechanism and influences of the polarization-induced electric field on the PCE have been discussed.

Results and Discussion

Polarization-induced electric field. Ferroelectric materials have spontaneous polarization without the need of an external electric field. The spontaneous polarization charges can be presented as $\sigma_{pol} = P n$, where P is the polarization vector and n is the unit normal to the surface. When a ferroelectric surface contacts with a conductive layer (i.e., ITO), polarization charges at the ferroelectric surface will be screened by free charges in the conductive layer. The distribution of screening charges in the conductive layer, very near the interface with the ferroelectric, leads to several important thickness-dependent electrical phenomena in ferroelectrics. A depolarization field can be formed due to the slight offset between the polarization charges at the ferroelectric surface and the screening charges in the conductive layer^{24–26}. Assume that the ferroelectric is homogeneously-poled, the interface states and space charge in the ferroelectric may be ignored²⁵, so that the polarization charges are localized at the ferroelectric/conductive-layer interface. The depolarization field (E_d) in the ferroelectric can be represented as

$$E_d = -\frac{P}{\epsilon_f} \left(\frac{2\epsilon_f/d}{2\epsilon_f/d + \epsilon_c/l_s} \right) \quad (1)$$

where d is the thickness of ferroelectric plate, l_s is the screening length (space charge extent in conductive layer), and ϵ_f and ϵ_c are the relative dielectric constants of the ferroelectric and the conductor, respectively²⁵. It is clear that the magnitude of the depolarization field is strongly plate thickness dependent. In our work, we used 0.3-mm-thick LiNbO₃ (i.e., $d = 0.3 \text{ mm}$) and 50 nm-thick ITO (which gives rise to $l_s = 0.05 \text{ nm}$)²⁷, i.e., $d \gg l_s$ and thus the depolarization field is predicted to disappear. In this case, screening charges reside at the ferroelectric/conductive-layer interface, completely compensating for the spontaneous polarization P in the ferroelectric. The screening charges (σ_s , $|\sigma_s| = |\sigma_{pol}|$), generates an electric field (E) within the adjacent TiO₂ layer, which is related to the polarization-induced electric field on the ferroelectric surface.

To verify the electric field induced by the spontaneous polarization of LiNbO₃ and whether it can penetrate through the ITO layer and TiO₂ film, surface potential properties of the photoanode after subjected to the sintering process were investigated with Kelvin probe force microscopy (KPFM). As shown in Fig. 2, surface potential of the TiO₂/ITO-LiNbO₃ (+Z, Fig. 2b) was much larger than that of the TiO₂/ITO-glass (Fig. 2c), indicating a

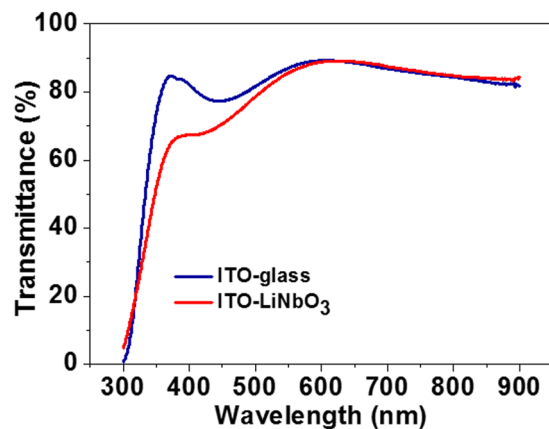


Figure 3. The UV-vis spectra of the collector electrodes of ITO-LiNbO₃ and ITO-glass.

potential enhancement on the TiO₂ film due to the employment of LiNbO₃. Topographic images (Fig. 2d and e) display a very similar morphology of TiO₂ nanoparticles for these two samples, suggesting that topography effect on the surface potential is negligible. The electric field generated from the LiNbO₃ at the tip scanning level can be estimated to be a few 10 V/μm. Variations of surface potential over the scan area were observed from both samples, which might be caused by an AC voltage generally applied to the tip while scanning. KPFM though is not for a quantitative measurement of surface potential²⁸, the results clearly confirmed that the electric field originating from the LiNbO₃ is significantly large and can penetrate through the ITO layer and TiO₂ film. In other words, the TiO₂ film is “immersed” in an electric field in view of the spontaneous polarization of LiNbO₃.

To demonstrate that the polarization-induced electric field can be introduced into DSCs for charge transport promotion, two types of cells were fabricated and studied in this work: ferro-based cell has a configuration of TiO₂/ITO-LiNbO₃ (+Z), while glass-based cell is composed of TiO₂/ITO-glass. For each type, more than five cells were adopted for characteristics of charge transport properties and photovoltaic performance.

Optical transmittance of collector electrodes. Optical properties of ITO-LiNbO₃ and ITO-glass were measured and compared, and their UV-vis transmittance spectra were shown in Fig. 3. It was found that both electrodes have good optical transmittance in the effective absorption wavelength region of N719, although the collector electrode of ITO-LiNbO₃ shows a lower transmittance at the wavelength range of 320–600 nm.

Charge transport properties. Effects of polarization-induced electric field on the charge transport properties in the DSCs were investigated by electrochemical impedance spectroscopy (EIS). As a well-established technique, the EIS has been widely employed to study the kinetics of electrochemical and photoelectrochemical systems including DSCs^{29–32}. Under the EIS measurement with a forward bias in dark, electrons are injected into the conduction band of TiO₂ nanoparticles from the collector electrode and then transported through the mesoscopic TiO₂ network. At the same time, some of the injected electrons react with I₃[−] in the electrolyte, which is related to the recombination process. The Nyquist plot typically consists of two semicircles, which is fitted by an equivalent circuit inserted in Fig. 4(a). The first small semicircle corresponds to the charge transfer resistance at counter electrode/electrolyte interface (R_1) at a high frequency ($>10^3$ Hz). The second large semicircle corresponds to the charge transport resistance within the TiO₂ film (R_t) at 10^3 – 10^2 Hz and the charge transfer resistance at the TiO₂/electrolyte interface (R_{ct}) around 10^1 Hz. R_t denotes how effective the electrons in the conduction band of TiO₂ network move along with the TiO₂ network, while R_{ct} reflects the charge recombination³³. Under the open circuit condition (V_{oc}), a relatively high carrier density results in a low diffusion resistance, the R_t is not usually detected in Nyquist plot due to its small value compared to other two charge transfer resistances R_1 and R_{ct} ³⁴. Therefore, the second large semicircle is mainly attributed to the charge transfer resistance R_{ct} .

Figure 4 shows the representative results of EIS measurements at the V_{oc} . An increase of R_{ct} was obtained from the ferro-based cell with the use of LiNbO₃ as shown in Fig. 4a. The larger the amount of R_{ct} , the more difficult the recombination of the electrons and holes, which results in decreased charge recombination^{35,36}. Figure 4b shows the Bode plots of the cells, indicating a longer lifetime for the ferro-based cell (32 ms) than the glass-based cell (24 ms). The electron lifetime (τ) can be determined by using the curve peak of the spectrum following equation³⁷:

$$\tau = \frac{1}{2\pi f_{peak}} \quad (2)$$

where f_{peak} is the peak frequency at the minimum phase angle, 4.915 Hz for the ferro-based cell and 6.478 Hz for the glass-based cell. Both the increases in the R_{ct} and τ lead to a reduced interface charge recombination in ferro-based cells.

Figure 4c displays J - V curves of the cells measured under dark conditions, showing dark currents caused by the reaction of injected electrons with I₃[−] in the electrolyte³⁸. The dark current was smaller in the ferro-based cell

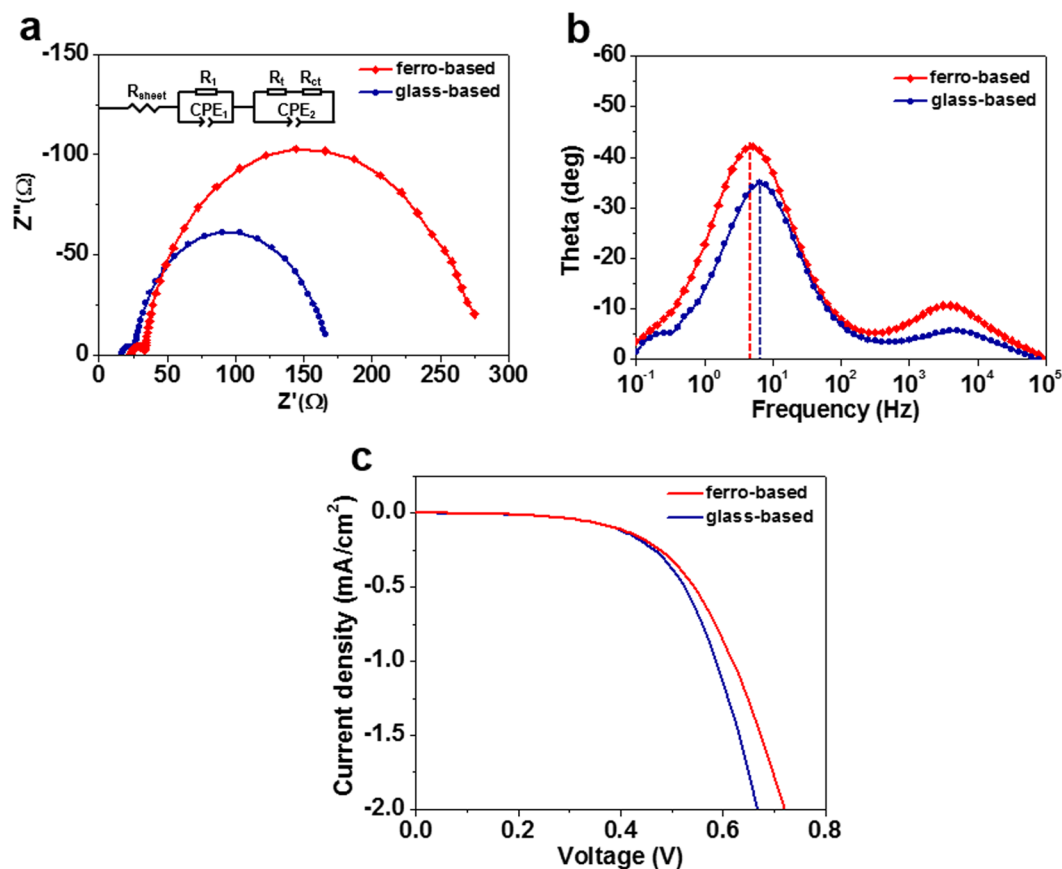


Figure 4. (a) Nyquist plot and (b) Bode plot of the ferro-based and glass-based cells under open circuit condition (V_{oc}), and (c) photocurrent density-voltage ($J-V$) curves of the ferro-based and glass-based cells under dark conditions.

than that in the glass-based cell. This is in keeping with the EIS results, which further demonstrates that charge recombination was impeded by the polarization-induced electric field in ferro-based cells.

Photovoltaic performance. Figure 5 shows the photocurrent density-voltage ($J-V$) characteristics and the corresponding incident monochromatic photon-to-electric current conversion efficiency (IPCE) spectra of the ferro-based and glass-based cells, and their photovoltaic performance parameters are summarized in Table 1. Ferro-based cell had a PCE of 4.46%, which is 42.9% higher than that of 3.12% for glass-based cell. Such an efficiency enhancement in ferro-based cells was mainly attributed to the increased J_{sc} . It is known that J_{sc} is the integration of the IPCE over the absorption range. As expected, ferro-based cells show higher IPCE values comparing with glass-based cells, despite the lower optical transmittance in LiNbO_3 , which is in a same trend to that of J_{sc} . The increased J_{sc} can be ascribed to the existence of a polarization-induced electric field from ferroelectric LiNbO_3 in the ferro-based cell, in which electrons transport along the TiO_2 network are enforced by the electric field toward the electron collection electrode and consequently the transport involves less charge recombination at the $\text{TiO}_2/\text{electrolyte}$ interfaces (Fig. 5d), resulting in a larger photocurrent density.

In addition to the increase in J_{sc} , fill factor (FF) of ferro-based cells also increases and contributes to the higher PCE. The FF reflects electrical and electrochemical losses occurring during operation of the DSC, it can be contributed by series and shunt resistance in the device. The shunt resistance (R_{sh}) is for the resistance related to the back electron transfer across the $\text{TiO}_2/\text{electrolyte}$ interface³⁹, and the series resistance (R_s) is mainly attributed to the sheet resistance of TCO substrates. Increasing R_{sh} and decreasing R_s will lead to a higher FF , thus resulting in a greater efficiency. The R_{sh} and R_s can be obtained by calculating the inverse of the slopes of $J-V$ characteristics near J_{sc} and V_{oc} , respectively. Compared with the glass-based cell, the ferro-based cell presents a slightly smaller R_s but an apparently larger R_{sh} , resulting in a larger FF (Table 1). The larger R_{sh} originating from reduced charge recombination can be ascribed to the field-assisted charge collection which leads to less opportunities for the electrons to back react at the $\text{TiO}_2/\text{electrolyte}$ interfaces. It should also be noted that the overall PCEs are not high due to the small FF . The large R_s caused by the ITO might be the reason for the small FF . To confirm this speculation, resistivity of the ITO and FTO (commonly used as a TCO of collector electrodes in DSCs) before and after the sintering process were measured and compared. The results show that the resistivity of the ITO increased slightly after subjected to the sintering process (2.767 and 2.865 $\Omega\cdot\text{cm}$ respectively, before and after sintering), however, it is 2.2 times of that of FTO (1.293 $\Omega\cdot\text{cm}$ after the same sintering process). The comparatively large resistivity of the ITO leads to the small FF thus the overall low PCEs from this work.

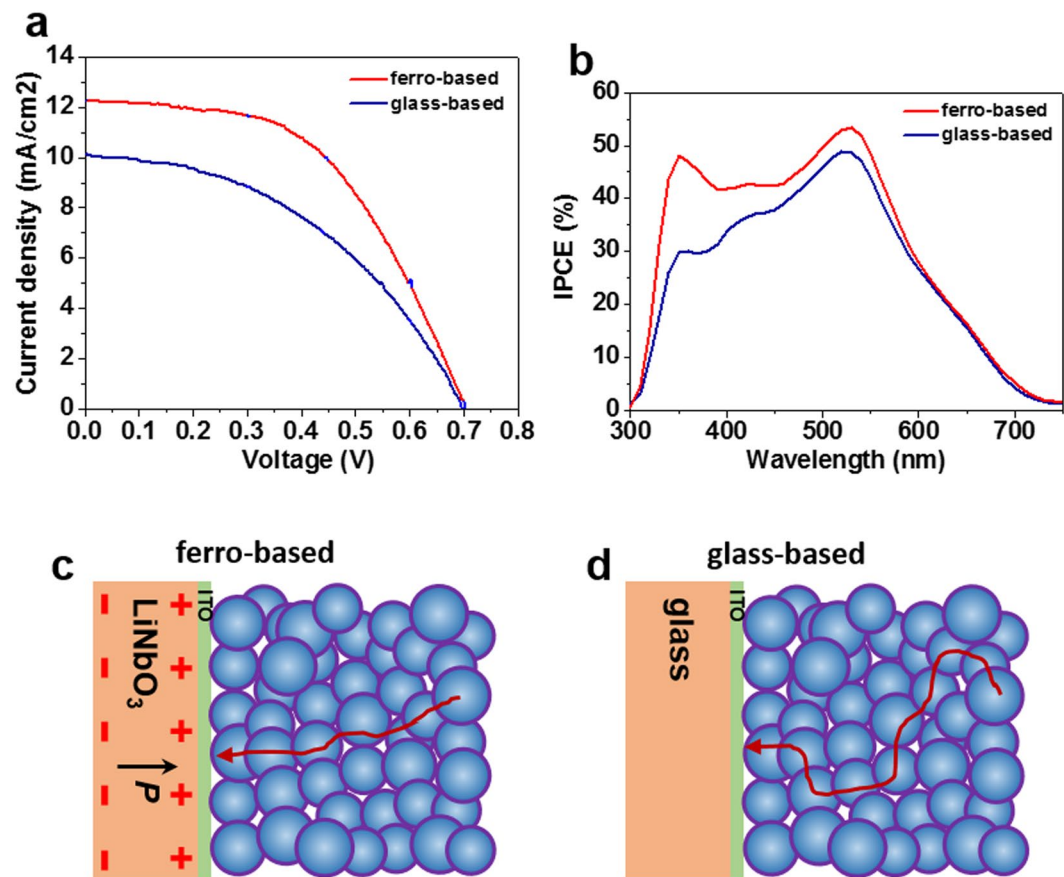


Figure 5. (a) Photocurrent density-voltage (J - V) curves and (b) incident photon-to-current conversion efficiency (IPCE) spectra of the ferro-based and glass-based cells under AM 1.5 with 100 mW/cm^2 . Schematics illustrating electron transport through the TiO_2 network in ferro-based (c) and glass-based (d) cells.

| device | J_{sc} (mA/cm ²) | V_{oc} (V) | FF | η (%) | R_s (k Ω cm ²) | R_{sh} (k Ω cm ²) |
|-------------|--------------------------------|--------------|------|------------|-------------------------------------|--|
| ferro-based | 12.27 | 0.7 | 0.52 | 4.46 | 0.0210 | 0.522 |
| glass-based | 11.12 | 0.7 | 0.44 | 3.12 | 0.0278 | 0.232 |

Table 1. Photovoltaic performance parameters of ferro-based and glass-based cells.

Conclusions

In summary, we report ferroelectric functionalized DSCs, in which a positively-poled LiNbO_3 single crystal coated with ITO was used as a collector electrode, have better performance due to higher photocurrent density and fill factor. The large spontaneous polarization of LiNbO_3 generates an electric field that can penetrate through the ITO layer and into TiO_2 film, giving rise to two impacts on electron transport in the mesoporous TiO_2 network: enhanced photocurrent density by attracting electrons to transport through the mesoporous TiO_2 network toward the collector electrode and decreased recombination chance by facilitating electrons to pass through fewer boundaries of TiO_2 nanoparticles. Further work is necessary to optimize the incorporation of ferroelectrics into solar cells in order to take full advantages of polarization-induced electric field to further enhance the PCE of DSCs.

Materials and Methods

Preparation of collector electrodes. LiNbO_3 single crystal of congruent composition (YAMAJYU Ceramics Co., Ltd, Japan) was uniformly poled along with the crystallographic Z-axis and cut perpendicular to the polar axis, and then polished to a plate with the thickness of 0.3 mm. Following the polishing, the plate was diced into $2 \times 2 \text{ cm}$ pieces and ultrasonic cleaned in acetone, methanol and deionized (DI) water sequentially, and then blown dry with nitrogen. After cleaning, a 50-nm-thick indium tin oxide (ITO) film was sputtered onto the positively-poled (+Z) surface of LiNbO_3 single crystals. For comparison, ITO-coated glasses were also prepared following the same process.

Fabrication of solar cells. TiO_2 paste was prepared based on the literature⁴⁰ using commercial TiO_2 powder (P25). Doctor-blading method was adopted to make a TiO_2 film onto the ITO- LiNbO_3 or ITO-glass. The film was

first dried at 150 °C for 30 min and then annealed at 350 °C for 1 h at the heating rate of 10 °C/min to remove the organic additives and to create a mesoporous network of TiO₂. Owing to the thermal restriction of ITO, 350 °C for 1 hr was applied to anneal the TiO₂ films in this work. It has been confirmed that, the organic residues can be entirely removed, and anatase TiO₂ phase structure can be formed after annealing at 350 °C⁴¹.

The resulting TiO₂ film was then sensitized with a 0.3 mM solution of N719 dye (Solaronix) for 24 h. The N719 dye was dissolved in ACN and tBA (volume ratio of 1:1) as a standard dye solution. The sensitized film was assembled with a counter electrode made of a Pt-coated silicon after removing excess dye with ethanol and drying with air flow. A 30- μ m-thick spacer was used to separate the sensitized film and the counter electrode, and the gap between them was filled with an electrolyte composed of 0.6 M tetrabutylammomium iodide, 0.1 M lithium iodide, 0.1 M iodine and 0.5 M 4-tert-butylpyridine in acetonitrile.

Characterization. The morphology of the glass, LiNbO₃, ITO-glass and ITO-LiNbO₃ (Figure S2) was characterized by atomic force microscopy (AFM, Asylum Research Cypher S) at an ac mode. The surface potential properties of TiO₂ film coated on collector electrodes after the sintering process were characterized by Kelvin probe force microscopy (KPFM, Asylum Research Cypher S), the corresponding surface morphology of the films can be obtained simultaneously with the KPFM. A conductive cantilever with a spring constant of 2 N/m and tip radius of 10 nm was used. Surface potential properties were characterized by scanning the TiO₂ films with the conductive tip at a constant level of 50 nm from the film.

The optical transmittance of the LiNbO₃ (Figure S1), ITO-glass and ITO-LiNbO₃ was characterized by UV-vis spectrometer. Electrochemical impedance spectroscopy (EIS) was performed using a Solartron 1287 A equipped with a Solartron 1260 FRA/impedance analyzer to investigate charge transport properties in the DSCs. The frequency range was set from 10⁻¹ to 10⁵ Hz and the oscillation potential amplitude was 10 mV. The photovoltaic performance of the DSCs was characterized by using a HP 4155 A programmable semiconductor parameter analyzer equipped with an AM 1.5 simulated sunlight with a power density of 100 mW/cm². The incident monochromatic photon-to-electron conversion efficiency (IPCE) plotted as a function of excitation wavelength were recorded on a QTest Station 1000 ADI system (Crowntech, Inc.) equipped with a 300 W Xe lamp. The monochromatic photocurrent-wavelength measurements were carried out by placing a monochromator, assisted by an automatic filter wheel, between the DSCs and the light source. A mask was used to enable an illuminated active area of 0.196 cm².

References

1. Yue, J. Y. *et al.* Enhanced photovoltaic performances of the dye-sensitized solar cell by utilizing rare-earth modified tin oxide compact layer. *Org Electron* **43**, 121–129 (2017).
2. Feng, K. Y. *et al.* Ferroelectric BaTiO₃ dipole induced charge transfer enhancement in dye-sensitized solar cells. *J Power Sources* **350**, 35–40 (2017).
3. Zhang, Q. F. & Cao, G. Z. Nanostructured photoelectrodes for dye-sensitized solar cells. *Nano Today* **6**, 91–109 (2011).
4. Meyer, G. J. The 2010 Millennium Technology Grand Prize: Dye-Sensitized Solar Cells. *Acc Nano* **4**, 4337–4343 (2010).
5. Nazeeruddin, M. K. *et al.* Conversion of Light to Electricity by Cis-X₂bis(2,2'-Bipyridyl-4,4'-Dicarboxylate)Ruthenium(II) Charge-Transfer Sensitizers (X = Cl-, Br-, I-, Cn-, and Scn-) on Nanocrystalline TiO₂ Electrodes. *J Am Chem Soc* **115**, 6382–6390 (1993).
6. Wang, M., Chen, P., Humphry-Baker, R., Zakeeruddin, S. M. & Gratzel, M. The Influence of Charge Transport and Recombination on the Performance of Dye-Sensitized Solar Cells. *Chemphyschem* **10**, 290–299 (2009).
7. Konenkamp, R. Carrier transport in nanoporous TiO₂ films. *Phys Rev B* **61**, 11057–11064 (2000).
8. Kopidakis, N., Schiff, E. A., Park, N. G., van de Lagemaat, J. & Frank, A. J. Ambipolar diffusion of photocarriers in electrolyte-filled, nanoporous TiO₂. *J Phys Chem B* **104**, 3930–3936 (2000).
9. Bisquert, J., Zaban, A. & Salvador, P. Analysis of the mechanisms of electron recombination in nanoporous TiO₂ dye-sensitized solar cells. Nonequilibrium steady-state statistics and interfacial electron transfer via surface states. *J Phys Chem B* **106**, 8774–8782 (2002).
10. Shen, Y., Nonomura, K., Schlettwein, D., Zhao, C. & Wittstock, G. Photoelectrochemical kinetics of eosin Y-sensitized zinc oxide films investigated by scanning electrochemical microscopy. *Chem-Eur J* **12**, 5832–5839 (2006).
11. Bisquert, J. Physical electrochemistry of nanostructured devices. *Phys Chem Chem Phys* **10**, 49–72 (2008).
12. Hailu, Y. M., Shie, W. R., Nachimuthu, S. & Jiang, J. C. New Insights into Organic Dye Regeneration Mechanism in Dye Sensitized Solar Cells: A Theoretical Study. *Acc Sustain Chem Eng* **5**, 8619–8629 (2017).
13. Vittal, R. & Ho, K. C. Zinc oxide based dye-sensitized solar cells: A review. *Renew Sust Energ Rev* **70**, 920–935 (2017).
14. Hwang, D. K., Nam, J. E., Jo, H. J. & Sung, S. J. Quasi-solid state electrolyte for semi-transparent bifacial dye-sensitized solar cell with over 10% power conversion efficiency. *J Power Sources* **361**, 87–95 (2017).
15. Park, K., Zhang, Q. F., Xi, J. T. & Cao, G. Z. Enhanced charge transport properties by strengthened necks between TiO₂ aggregates for dye sensitized solar cells. *Thin Solid Films* **588**, 19–25 (2015).
16. Snaith, H. J. Estimating the Maximum Attainable Efficiency in Dye-Sensitized Solar Cells. *Adv Funct Mater* **20**, 13–19 (2010).
17. Yuan, Y. B. *et al.* Efficiency enhancement in organic solar cells with ferroelectric polymers. *Nat Mater* **10**, 296–302 (2011).
18. Nalwa, K. S. *et al.* Enhanced charge separation in organic photovoltaic films doped with ferroelectric dipoles. *Energ Environ Sci* **5**, 7042–7049 (2012).
19. Lan, J. L. *et al.* The effect of SrTiO₃:ZnO as cathodic buffer layer for inverted polymer solar cells. *Nano Energy* **4**, 140–149 (2014).
20. Kim, H. S. *et al.* Ferroelectric Polarization in CH₃NH₃PbI₃ Perovskite. *J Phys Chem Lett* **6**, 1729–1735 (2015).
21. Gopalan, V., Mitchell, T. E., Furukawa, Y. & Kitamura, K. The role of nonstoichiometry in 180 degrees domain switching of LiNbO₃ crystals. *Appl Phys Lett* **72**, 1981–1983 (1998).
22. Liu, X. Y., Kitamura, K. & Terabe, K. Surface potential imaging of nanoscale LiNbO₃ domains investigated by electrostatic force microscopy. *Appl Phys Lett* **89** (2006).
23. Liu, X. Y., Terabe, K. & Kitamura, K. Surface potential properties on near-stoichiometric LiNbO₃ crystals with nanoscale domain-engineered structures. *J Electroceram* **16**, 399–402 (2006).
24. Junquera, J. & Ghosez, P. Critical thickness for ferroelectricity in perovskite ultrathin films. *Nature* **422**, 506–509 (2003).
25. Mehta, R. R., Silverman, B. D. & Jacobs, J. T. Depolarization Fields in Thin Ferroelectric Films. *J Appl Phys* **44**, 3379–3385 (1973).
26. Kornev, I., Fu, H. X. & Bellaiche, L. Ultrathin films of ferroelectric solid solutions under a residual depolarizing field. *Phys Rev Lett* **93** (2004).
27. Kim, D. J. *et al.* Polarization relaxation induced by a depolarization field in ultrathin ferroelectric BaTiO₃ capacitors. *Phys Rev Lett* **95** (2005).
28. Wen, H. F. *et al.* Investigation of tunneling current and local contact potential difference on the TiO₂(110) surface by AFM/KPFM at 78 K. *Nanotechnology* **28** (2017).

29. Bisquert, J. Theory of the impedance of electron diffusion and recombination in a thin layer. *J Phys Chem B* **106**, 325–333 (2002).
30. Bisquert, J. & Vikhrenko, V. S. Interpretation of the time constants measured by kinetic techniques in nanostructured semiconductor electrodes and dye-sensitized solar cells. *J Phys Chem B* **108**, 2313–2322 (2004).
31. Han, L. Y., Koide, N., Chiba, Y. & Mitate, T. Modeling of an equivalent circuit for dye-sensitized solar cells. *Appl Phys Lett* **84**, 2433–2435 (2004).
32. Wang, Q. *et al.* Characteristics of high efficiency dye-sensitized solar cells. *J Phys Chem B* **110**, 25210–25221 (2006).
33. Lv, Q. *et al.* Promotion effect of TiO₂ on catalytic activity and stability of Pt catalyst for electrooxidation of methanol. *J Power Sources* **218**, 93–99 (2012).
34. Hoshikawa, T., Yamada, M., Kikuchi, R. & Eguchi, K. Impedance analysis of internal resistance affecting the photoelectrochemical performance of dye-sensitized solar cells. *J Electrochem Soc* **152**, E68–E73 (2005).
35. van de Lagemaat, J., Park, N. G. & Frank, A. J. Influence of electrical potential distribution, charge transport, and recombination on the photopotential and photocurrent conversion efficiency of dye-sensitized nanocrystalline TiO₂ solar cells: A study by electrical impedance and optical modulation techniques. *J Phys Chem B* **104**, 2044–2052 (2000).
36. Kern, R., Sastrawan, R., Ferber, J., Stangl, R. & Luther, J. Modeling and interpretation of electrical impedance spectra of dye solar cells operated under open-circuit conditions. *Electrochim Acta* **47**, 4213–4225 (2002).
37. Bisquert, J., Fabregat-Santiago, F., Mora-Sero, L., Garcia-Belmonte, G. & Gimenez, S. Electron Lifetime in Dye-Sensitized Solar Cells: Theory and Interpretation of Measurements. *J Phys Chem C* **113**, 17278–17290 (2009).
38. Ito, S. *et al.* Control of dark current in photoelectrochemical (TiO₂/I⁻/I₃⁻) and dye-sensitized solar cells. *Chem Commun (Camb)*, 4351–4353, <https://doi.org/10.1039/b505718c> (2005).
39. Gratzel, M. Photoelectrochemical cells. *Nature* **414**, 338–344 (2001).
40. Ito, S. *et al.* Fabrication of screen-printing pastes from TiO₂ powders for dye-sensitized solar cells. *Prog Photovoltaics* **15**, 603–612 (2007).
41. Xi, J., Dahoudi, N. A., Zhang, Q., Sun, Y. & Cao, G. Effect of annealing temperature on the performances and electrochemical properties of TiO₂ dye-sensitized solar cells. *Science of Advanced Materials* **4**, 727–733 (2012).

Acknowledgements

This work was supported by the National Natural Science Foundation of China (51472037) and Shenzhen Science and Technology Innovation Committee (JCYJ20170818160815002). J.Y. Li also acknowledges support from the National Key Research and Development Program of China (2016YFA0201001) and Natural Science Foundation of Guangdong Province (2017A030313342).

Author Contributions

X.Y.L. designed the study, interpreted the data, and wrote the main manuscript text. G.Z.C. and Q.F.Z. interpreted the data and wrote the part of manuscript text. X.T. carried out the impedance experiments. J.Y.L. and N.V. made a great contribution in the process of revise the manuscript.

Additional Information

Supplementary information accompanies this paper at <https://doi.org/10.1038/s41598-018-35764-y>.

Competing Interests: The authors declare no competing interests.

Publisher's note: Springer Nature remains neutral with regard to jurisdictional claims in published maps and institutional affiliations.



Open Access This article is licensed under a Creative Commons Attribution 4.0 International License, which permits use, sharing, adaptation, distribution and reproduction in any medium or format, as long as you give appropriate credit to the original author(s) and the source, provide a link to the Creative Commons license, and indicate if changes were made. The images or other third party material in this article are included in the article's Creative Commons license, unless indicated otherwise in a credit line to the material. If material is not included in the article's Creative Commons license and your intended use is not permitted by statutory regulation or exceeds the permitted use, you will need to obtain permission directly from the copyright holder. To view a copy of this license, visit <http://creativecommons.org/licenses/by/4.0/>.

© The Author(s) 2018